Sensors & Diagnostics

PAPER

Check for updates

Ultra-low dual detection of tetrahydrocannabinol and cannabidiol in saliva based on electrochemical sensing and machine learning: overcoming cross-interferences and saliva-to-saliva variations†

Greter A. Ortega,‡ Herlys Viltres, [iD] ‡ Hoda Mozaffari, Syed Rahin Ahmed, Seshasai Srinivasan [iD] * and Amin Reza Rajabzadeh [iD] *

A novel alternative to cope with saliva-to-saliva variations and cross-interference while sensing delta-9-tetrahydrocannabinol (THC) and cannabidiol (CBD) is reported here using two voltammetric sensors coupled with machine learning. The screen-printed electrodes modified with the same analyte molecules (m-Z-THC and m-Z-CBD) were employed for sensing ultra-low concentrations of THC and CBD in the 0 to 5 ng mL^{-1} range in real human saliva samples. Simultaneous detection of THC and CBD was carried out using m-Z-THC or m-Z-CBD to study the performance of each modified sensor. Also, CBD and THC have the same molecular structure; there is only a slight difference in how the atoms are arranged, and therefore both molecules will have similar electrochemical performance. Consequently, CBD can be a potential interference while detecting THC and THC can be an interference during CBD detection using electrochemical sensors. Therefore, machine learning was introduced to analyze the sensor analytical responses to overcome such issues. The data processing results provide suitable accuracies of 100% for training in the case of both sensors and 92 and 83% for m-Z-THC and m-Z-CBD, respectively, for dataset testing THC and CBD in saliva samples. Additionally, the saliva samples containing CBD and THC as cross-interference were accurately identified and classified.

1. Introduction

Electrochemical detection of coexisting analytes with similar structure interferents is a significant problem in chemical sensors. For example, Δ9-tetrahydrocannabinol (THC), which is the main psychoactive of cannabis, is currently traceable in saliva samples by using electrochemical sensors.[1] However, cannabis-based medicine can now be prescribed for medicinal use in many countries, comprising both THC and the familiar component cannabidiol (CBD).[2]

The previous work published by the authors of this article reported an innovative electrochemical-based sensor to detect ultra-low Δ9-tetrahydrocannabinol (THC) in saliva.[3] The carbon-based working electrode (WE) was modified in the

School of Engineering Practice and Technology, McMaster University, 1280 Main Street West, Hamilton, ON, L8S 4L8, Canada. E-mail: ssriniv@mcmaster.ca, rajaba@mcmaster.ca

† Electronic supplementary information (ESI) available. See DOI: https://doi.org/10.1039/d4sd00102h

‡ G. Ortega and H. Viltres have equal contribution as first author.

sensor fabrication by electrodeposition of the same analyte to be detected later in the sample using square wave voltammetry (SWV). Nevertheless, while THC presents a phenol group, oxidizable at potentials near 0.4 V, CBD arranges two aromatic *meta*-hydroxyl groups with the same oxidizable capability at almost the same potential as THC. Hence, CBD is a substantial interferent during the detection of THC by electrochemistry.

Nowadays, strategies have been implemented to overcome interferences during electrochemical testing. Overall, some of them reported for THC and CBD detection[4] are pre-treatment procedures that encompass solid-phase extraction,[5] paper chromatography,[6] or other separation methods;[7] molecularly imprinted nanoparticles (nanoMIPs);[8] working electrode modifications with macrocyclic compounds[9] and suitable (nano)materials.[10] In other cases, two different methodologies have been applied to prevent the interferences because of the adsorption of oxidation products, such as pH optimization and the pre-treatment of the electrode through a cathodic potential step.[11] However, all these strategies are ineffective in detecting an ultra-low concentration of THC in the presence of CBD under practical sensor conditions and in a short time.

Furthermore, many challenges have not been fully addressed in the literature for saliva sensors due to the complexity of the nature of saliva.[12–14] Human saliva is a complex matrix with a viscosity of approximately 1.30 times higher than that of water, affecting the analyte's diffusion and the reaction rates on the electrodes.[13,14] In addition, saliva has various natural or adulterant electroactive components that may interfere with the electrochemical performance of the analyte. Furthermore, the pH, conductivity, and protein–chemical–solid compositions of saliva, among others, change over time and vary from person to person. For all the reasons mentioned, obtaining consistent responses during the electrochemical testing of chemical sensors is incredibly problematic.

Machine learning (ML) algorithms offer exceptional solutions to complex and large-size data systems involving problems that traditionally require tedious hand-tuning rules and tasks with fluctuating environments.[15] ML refers to computational techniques that learn from past experiences, *i.e.*, data, to create logical and precise prediction algorithms. The data used in these learning algorithms play a crucial role in the success of ML models; hence, ML is the intersection of data analysis and statistics with computer programming.[16]

Some reports have implemented ML algorithms coupled with different analytical techniques to detect an assortment of analytes in the past years. Some examples are fluorescence,[17] colorimetry,[18] colour-based lateral flow test,[19] ion-mobility spectrometry (IMS), and photoionization detection comprising electrochemical-based sensors (PIDECS),[20] transcriptomics and proteomics data,[21] Fourier transform infrared spectroscopy (FTIR),[22,23] and electrochemical sensors.[24] Table S1, provided in the ESI,† presents a summary of the reports dealing with ML in electrochemical sensors. In THC detection, few reports deal with ML during data set analysis; one used a chemiresistor[25] and the other used impedance.[26] Recently Rao *et al.*[27] studied the detection of a broad range of dopamine concentrations (9–200 μM) in the presence of a similar structure molecule epinephrine (EP) in PBS and blood and urine diluted 100 times in PBS (to eliminate the matrix effect) by implementing ML techniques sequentially. They used dual-modal sensors and selective features to feed the proposed ML algorithm. The focus of this work, however, is to detect ultra-low concentrations of cannabis in real samples (real saliva) in the presence of similar structures *via* feeding different ML algorithms separately with the entire voltammetry signals. Given the similar molecular structures of CBD and THC, which lead to comparable electrochemical performance and potential cross-interference, the novelty of this work lies in the dual detection of THC and CBD, differentiating their concentrations and addressing their cross-interferences while mitigating saliva-to-saliva variations. Table S2 is provided in the ESI† for details.

This paper reports on the development of two sensors to detect THC and CBD in real saliva. This work also introduces ML to analyze the data sets obtained from the electrochemical THC and CBD sensors to overcome the person-to-person variation setbacks and the cross-interference problems in complex saliva samples.

2. Materials and methods

For the purposes of this research, saliva samples from healthy humans in the lab, the authors, were used in this study. The screen-printed electrodes (SPE), TE100, employed in this study were obtained from Zensor R&D and comprise working (3 mm/0.071 cm^2) and counter carbon electrodes and a silver reference electrode (TE100). From now on, Zensor will be used to refer to SPEs. The reagents (−)-*trans*-Δ^9-tetrahydrocannabinol (THC) and cannabidiol (CBD) were obtained from Cerilliant-Sigma-Aldrich as standard solutions in methanol (ampule of 1 mg mL^{-1}) with the appropriate certification for laboratory uses. An ELISA THC Oral Fluid Kit Product (no. 120519) was acquired from Neogen Corporation.

Electrochemical analyses were carried out using a mono-potentiostat PalmSens4 with the PSTrace 5-Palm-Sens software. Samples were analyzed by performing Fourier transform infrared (FTIR) spectroscopy using a micro-attenuated total reflectance (micro-ATR) accessory equipped with a germanium crystal under a Hyperion 2000 microscope incorporated into a Bruker Tensor II spectrometer. XPS analyses were performed using a Kratos AXIS Supra X-ray photoelectron spectrometer with a monochromatic Al K(alpha) source (15 mA, 15 kV). The work function of the spectrometer was calibrated to the Au 4f$_{7/2}$ line for metallic gold with a binding energy (BE) of 83.96 eV, and the dispersion of the equipment was regulated to the Cu 2p$_{3/2}$ line of metallic copper with a BE of 932.62 eV. An analysis area of 300 × 700 microns and a pass energy of 160 eV were the conditions used to collect the survey scans. High-resolution analyses were performed using an analysis area of 300 × 700 microns and a pass energy of 20 eV. The spectra were charged and corrected to the C–C, C–H line of the carbon 1 s spectrum (aliphatic carbon) set to 285.00 eV and analyzed using the CasaXPS software (version 2.3.14).

2.1. Electrochemical sensors

In the THC-based sensor, the working electrode was modified with THC molecules (m-Z-THC), and in the case of the CBD-based sensor, with CBD molecules (m-Z-CBD).

2.1.1. Manufacturing of the THC and CBD-modified Zensor electrodes. Before THC or CBD deposition, Zensor electrodes were cleaned using Milli-Q lab water and dried with a brief flow of hot air. After that, stock solutions of THC or CBD (50–150 μg mL^{-1}) were prepared by adding THC or CBD solution (1 mg mL^{-1} in methanol) to a mix of methanol/water. Subsequently, 1 μL of the stock solution was dropped onto the WE surface of the Zensor electrodes and allowed to dry at ambient temperature and in a warm air flow for 30 seconds and 5 seconds, respectively. The resultant modified electrodes comprised an initial THC (m-Z-THC) or CBD (m-Z-CBD) deposition of 130 and 100 ng, respectively. The

modified electrodes were then subjected to pre-treatment before their final application employing an electrochemistry method, square wave voltammetry (SWV), using 0.01 M PBS solution. The following conditions were employed to record the electrochemical measurement: 0.05 V and 0 s as the precondition potential, 3 s for the equilibration time, 0–0.8 V range for the voltammetric potential scan with a frequency of 15 Hz, 25 mV of amplitude, and 5 mV for the step potential. The SWV signals were recorded for all Zensor electrodes under study, and THCi or CBDi will be used to refer to these electrodes. Subsequently, the modified electrodes, m-Z THC and m-Z CBD, were carefully washed using Milli-Q lab water and kept at 4 °C with nitrogen gas.

2.1.2. Collection and treatment of the saliva samples. The saliva of the lab members was collected using 15–50 mL polypropylene tubes, which were sealed with parafilm. The saliva samples were then dispensed into 1.5 mL Eppendorf vials. The samples were spiked with an adequate amount of THC in 0.01 mL of methanol to obtain final concentrations of 0, 2, and 5 ng mL^{-1}. An absorbent material swab was introduced inside the vial to collect the sample. The swabs with the absorbed saliva were introduced within a device that contained an appropriate filter and then squeezed with a plunger. The filtered saliva samples were collected in another vial to be prepared for the testing. Table S3, provided in the ESI,† summarizes different swab providers and tested filters.

2.1.3. THC sensor performance. 50 μL of the THC samples previously spiked with methanol in a 9 : 1 ratio were added onto the m-Z-THC electrodes and immediately subjected to SWV using the subsequent conditions: 0.05 V for 30 s as a precondition potential, 3 s as the equilibration time, 0–0.8 V range for the voltammetric potential scan from and a frequency of 15 Hz, 25 mV as the amplitude, and 5 mV as the step potential. For traditional analysis, the current values corresponding to each concentration result from subtracting the intensity of the peaks for the samples recovered with m-Z-THC (sensing electrode) minus the signal obtained with the pristine electrode (pristine Zensor, p-Z).

2.1.4. CBD sensor performance. CBD in low concentration levels in methanol (0, 2, and 5 ng mL^{-1}) were spiked into the saliva samples. The saliva samples were collected and prepared following the protocol described in sections 2.1.2 and 2.1.3. Then, 50 μL of the CBD-spiked samples were dropped onto m-Z-CBD electrodes. Then, a SWV analysis is performed using the subsequent parameters: 0.05 V for 30 s as a precondition potential, 3 s as the equilibration time, 0–0.8 V for the voltammetric potential scan and a frequency of 15 Hz, 25 mV as the amplitude, and 5 mV as the step potential. After that, another 50 μL from the same CBD spiked sample was incorporated on the pristine Zensor and analyzed under the same electrochemical conditions employed for the m-Z-CBD measurement. The subtracting methodology was then employed.

2.1.5. Interference studies. The performance of the m-Z-THC sensor to detect THC in the presence of CBD was evaluated. Also, the ability of CBD detection by the m-Z-CBD sensor in the presence of THC was studied. The response for both sensors was recorded before and after adding increasing amounts of each compound to a solution comprising 0, 2, and 5 ng mL^{-1} THC or CBD using SWV employing the same working conditions outlined in section 2.1.3. Diverse experiments were carried out to evaluate the influence of CBD or THC on the electrochemical performance of the modified electrodes (m-Z-THC and m-Z-CBD) during the THC or CBD detection. Table S4, provided in the ESI,† describes the experiment in detail.

2.2. Machine learning algorithms

Principal component analysis and several ML techniques like random forest, artificial neural network, and support vector machine for dimensionality reduction were used to classify THC and CBD saliva samples with concentrations of 0, 2, and 5 ng mL^{-1}. The training dataset was divided into subspaces based on an attribute that offers maximum information gain. In all cases, the ratio of training to testing dataset was 4. In this study, the optimal number of random trees was 200. An artificial neural network (ANN) was also used in this study for the purposes of classification. The dense network structure used in this study consisted of three hidden layers with 32, 64, and 128 nodes, respectively. The rectified linear unit function was used for the activation of the hidden layers, and softmax for the output layer was implemented. Additionally, regularization techniques, as well as dropout, were executed. This study also used the support vector machine (SVM) as another alternative for classification and regression. In this case, a radial basis function kernel for classification and a moderate regularization parameter for regression were included.

A logistic regression classifier for binary classification of the interaction between THC and CBD was also evaluated. Lastly, this work used principal component analysis (PCA) for dimensionality reduction and different preprocessing techniques, including standard scaler and non-linear power transformer for feature scaling. In all cases, the cumulative explained variance of the transformed dataset covered 98% of the original datasets. A detailed explanation of each algorithm is described in the ESI† S2.2.

3. Results and discussion

3.1. Characterization of m-Z-THC and m-Z-CBD

Both sensors, the m-Z-THC and the m-Z-CBD developed in this study, were designed based on the hydroxyl group oxidation present in THC and CBD molecules during the application of a potential to create C═O moieties followed by the formation of quinones, adducts, or more complex structures (Fig. 1a).[28] The presence of THC or CBD species in the sensors (m-Z-THC and m-Z-CBD) enhanced further physical and chemical interactions of the working electrodes with the THC or CBD molecules present in the sample, hence the oxidation process. To determine the electrochemical behaviour of bare Zensor and modified Zensor electrodes,
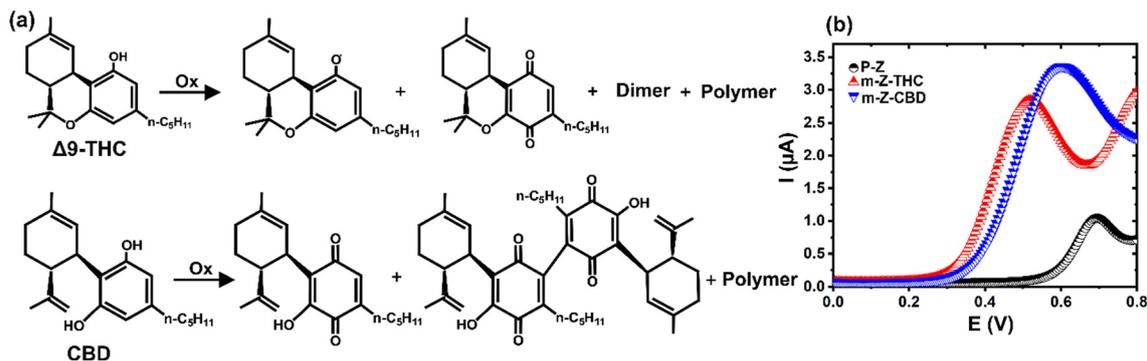
Fig. 1 a) Schematic representation of the oxidation of THC and CBD molecules. b) SWV response of THC-based (m-Z-THC, 130 ng) and CBD-based (m-Z-CBD, 100 ng) sensors in PBS.

SWV was performed in PBS solution. After modifying the pristine Zensor electrodes, an oxidation peak between 0.4 and 0.7 V appears in the m-Z-THC and the m-Z-CBD sensors (Fig. 1b). The peak related to m-Z-CBD appeared at slightly higher potentials compared to m-Z-THC.

On the other hand, FTIR and XPS characterization techniques were employed to study the pristine and modified electrode samples to get a deeper understanding of the surface of the electrode. In the FTIR spectrum (Fig. S1a†), the weak peaks in the 3000–2800 cm^{-1} region are correlated with the stretching vibration of C–H bonds for pristine and modified electrodes. The characteristic peak for the stretching of the O=C bond appears at approximately 1746 cm^{-1} in all samples (Fig. S1b,† zoom of the region 2000–1000 cm^{-1}). The signal at 1580 cm^{-1} can be assigned to the C=C bonds in aromatic ring structures, and the band at 1441 cm^{-1} was associated with the C–H bending mode. However, significant changes after pristine electrode modification were not possible to distinguish in the FTIR spectrum due to this technique's ability to sense the bulk material, not the surface. In this case, all chemical processes for Zensor electrode modification occur on the surface of the working electrode; therefore, the XPS technique was used to gain a clearer vision.

The XPS spectrum for the WE surface of pristine Zensor electrodes (p-Z) was obtained after dispensing THC or CBD (m-Z-THC_0 and m-Z-CBD_0) and SWV electrodeposition in PBS was the final manufacturing step. The survey spectra confirmed the existence of only C, O, N, Cl, S, and Si for all five samples and P in four of the samples (Table S5†). After pristine Zensor modification, the C and O atomic percent increased for both m-Z-THC and m-Z-CBD electrodes (Fig. 3a). In the case of the electrodes after dispensing m-Z-THC_0 and m-Z-CBD_0, the amount of C was observed to be slightly lower than that after the final electrodeposition step; meanwhile, the percent of O was found to be lower for the final sensors (m-Z-THC and m-Z-CBD). These changes in the sample's composition could be related to the interaction of the organic molecules with the working electrode surface and the formation of complex structures between the modifier molecules (Fig. 1a).

The C 1s high-resolution signal of the pristine sample was deconvoluted into four contributions at 284.4, 285.0, 286.5,

and 289.0 eV (Fig. 2b, Table S6†). The first contribution is related to aromatic C=C from graphitic carbon and ink employed for the working electrode preparation.[29] The signal at 285.0 eV was associated with C–C/C–H. The contributions at higher binding energies, 286.5 and 289.0 eV, were related to C–OH/C–O–C/C–Cl and O–C=O, respectively.[30,31] After pristine electrode modification with THC or CBD, no substantial variations were evidenced in the high-resolution C 1s signals for the other four samples (Fig. 2b and c and S2, Table S6†).

On the other hand, two contributions were observed in the O 1s spectra of all the samples. In the case of pristine modification, the first contribution at 532.5 eV was assigned to C=O.[30] The second peak was observed at higher binding energy, recorded at 533.5 eV for aromatic O*–(C=O)–C/C–O (Fig. 2e, Table S7†).[29] The O 1s for modified sensors showed a small shift (0.2–0.3 eV) to lower binding energy for the first contribution (Fig. 2f and g and S2; Table S7†). This might suggest slight changes in the O environment after pristine modification.

For the specific case of electrode modification with THC, a decrease and an increase of atomic percent for the first and second contributions, respectively, were observed in the O 1s fit when the modifier molecule was deposited onto the surface of the electrode (m-Z-THC_0) (Fig. 2h). After SWV analysis of m-Z-THC_0, the atomic percent of the C=O contribution increased; meanwhile, a decrease for O*–(C=O)–C/C–O was evidenced. These changes are related to the oxidation of the OH group to the quinones in the THC structure, which appears at 532.2 eV (C=O, first contribution).

A similar behaviour was evidenced for m-Z-CBD, where the atomic percent for the first peak of the O 1s fit in m-Z-CBD was found to be lower than in m-Z-THC and higher for the second peak. Additionally, the difference between both contributions in the m-Z-CBD sensor was significantly smaller than in the case of m-Z-THC because the CBD molecule has two OH groups present in the structure. However, one of these OH groups does not participate in the oxidation process. The XPS results corroborated that the element oxygen plays a substantial role in the electrochemical oxidation of THC and CBD molecules on the surface of the working electrode. Furthermore, the oxidation
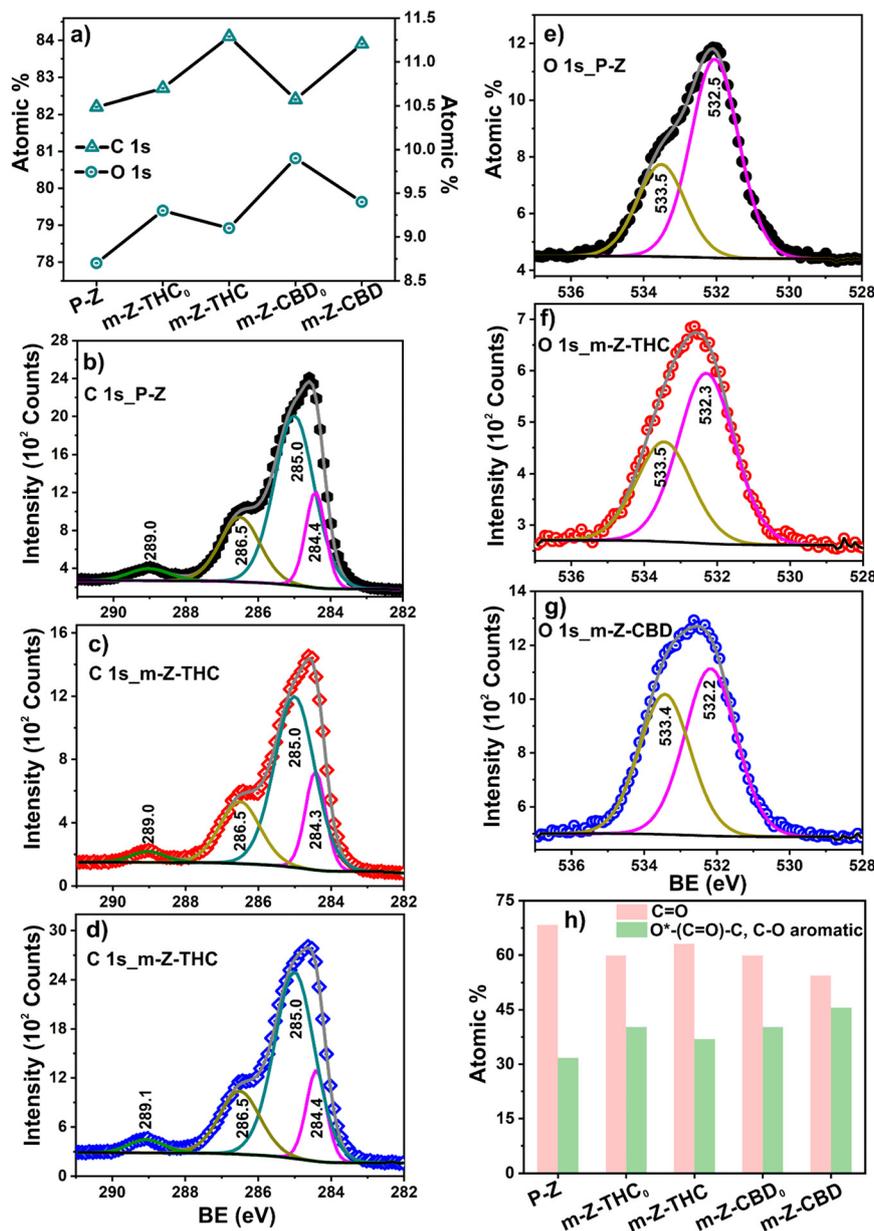
Fig. 2 a) Element quantification from survey spectra; b)–d) C1s and e)–g) O1s high-resolution spectra before and after Zensor working electrode modification. h) The ratio of the important functional groups from the high-resolution XPS spectra of O 1s of pristine and modified electrodes.

of OH groups in the modifier molecules to quinones after SWV of deposited electrodes with possible dimer and polymer formation was also confirmed.

3.2. Traditional analysis of the sensor performance

3.2.1. THC sensor performance with THC saliva samples. Saliva-to-saliva variations. As was explained earlier, the THC molecules (THCi) were first electrodeposited on the working electrode through SWV (Fig. 3a). Such molecules assisted the analyte–WE interaction and amplified the final SWV signal regarding the oxidation of the THC contained in the sample (Fig. 3b). Lastly, the values of the currents corresponding to each concentration result from subtracting the signals for the

samples recovered from the m-Zensor (sensing electrode) minus the signal obtained from the pristine Zensor (Fig. 3c). In traditional analysis, the intensity I regarding the baseline is directly correlated with the THC concentration present in the sample. In this sense, the biomolecule-free electrochemical approach helped to detect THC in PBS (1.1 ng mL^{-1}), simulated saliva (1.6 ng mL^{-1}), and real saliva (1.6 ng mL^{-1}).[3] Many experimental conditions were studied during the manufacturing, sample preparation, and sensor performance. During the THC detection in real saliva, the validation and recovery of this molecule were tested with suitable results for four real saliva samples using THC concentrations of 0, 2, and 5 ng mL^{-1}. Finally, the next step to evaluate the electrochemical approach proposed was testing with saliva samples from
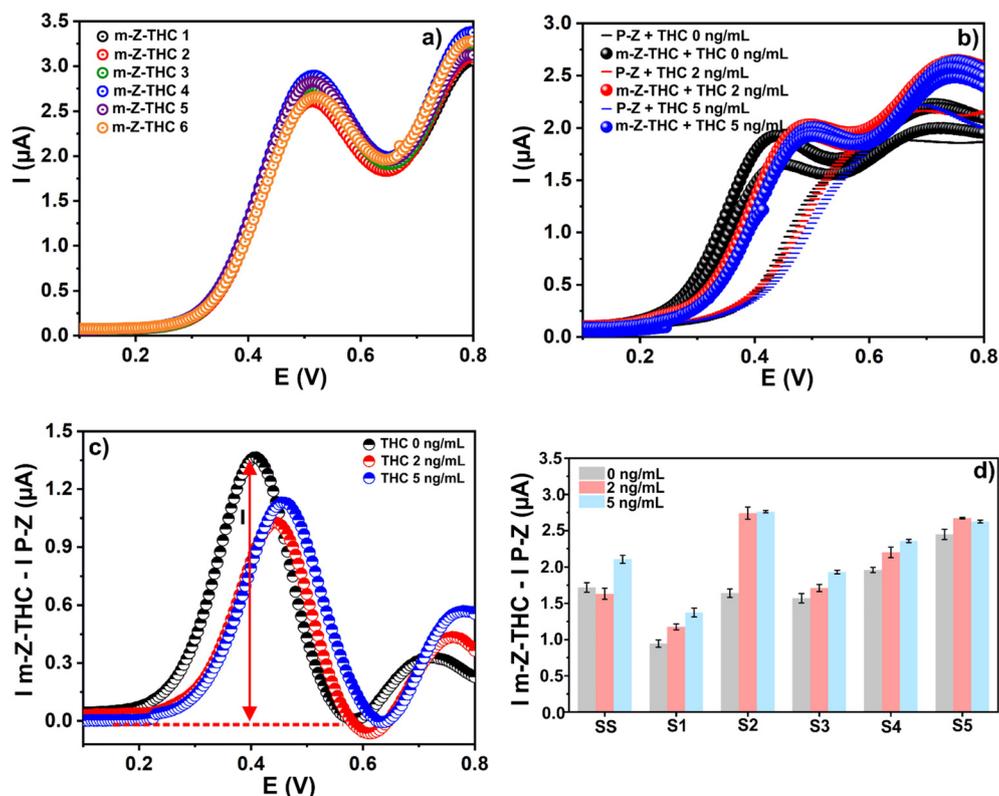
Fig. 3 a) SWV signals during the THC deposition of different modified electrodes (m-Z-THC). b) Raw data of 3 m-Z-THC and one pristine (p-Z) per THC concentration 0, 2, and 5 ng mL^{-1}. c) An example of the subtraction of signals for the samples (0, 2, and 5 ng mL^{-1} THC) recovered with m-Z-THC minus signals obtained with pristine Zensor. d) Sensor electrochemical performance using 130 ng of THCi and testing synthetic saliva (SS) and five real saliva samples (S1–S5) with 0, 2, and 5 ng mL^{-1} THC collected and filtered with OFCD-100 swab/glass wool.

various individuals since saliva has different properties and compositions.

Considering previous studies, saliva viscosity and natural conformation disturbed the electrode performance controlled by adsorption processes. In this sense, electroactive molecules, proteins such as mucin, or supernatant solids should be eliminated to decrease the variability among the results. It is important to mention that the THC concentration must be invariant in all processes. For this reason, an optimization of the saliva collection and filtration process was required. Table 1 summarizes the values of THC recoveries in saliva samples after being collected or filtered and quantified using the ELISA THC Oral Fluid Kit Product from Neogen Corporation.

Some collection or filtration systems provided high values of recoveries; however, they also presented some disadvantages. For example, the wwPTFE filter (0.2 μm) and POREX OFCD-201-SRF (with filter) helped clean the saliva but showed low volume recoveries. SalivaBio and POREX OFCD-100 were unsuccessful in cleaning, providing almost raw saliva. In contrast, the PureSal product was successful in cleaning the saliva; however, it resulted in a loss of THC in the swab. The SalivaBio Swab + PureSal filter interacted with the samples, leading to electrochemical interferences and a strong signal around 0.4 V, like THC. Lastly, the POREX OFCD-100 + glass wool successfully cleaned the saliva but was difficult to squeeze, compromising the volume recovery.

The best collection/filtration solution was the combination of the swab of the collector OFCD-100 and post-filtration using glass wool (Pyrex 9350). In this case, such a combination cleans the saliva samples, presents suitable volume recovery, and has no electrochemical interference. From this point, all experiments were performed using this strategy.

However, even after cleaning the saliva, there were inconsistencies in the results when comparing the current values of the same concentration but in different individual samples. For example, in Fig. 3d, the results show inconsistencies and unclear tendencies while testing different concentrations of THC.

3.2.2. CBD sensor performance with CBD saliva samples. Analogous to the THC sensor using m-Z-THC to detect THC saliva samples, modified electrodes with CBD (m-Z-CBD) were investigated with different saliva samples spiked with 0, 2, and 5 ng mL^{-1} CBD. The results were almost identical to THC (Fig. 4a), with slight variation in the features of the signals and an uncertain tendency of the current intensities to the CBD concentrations (Fig. 4b).

3.3. CBD and THC as interferences of the THC and CBD electrochemical sensors

The selectivity of the designed sensors was evaluated through the effect of CBD (THC) molecules in the determination of

Table 1 Results of the THC recoveries in saliva samples with 5 ng mL^{-1} THC after collection or filtration

Filters[a]		Collectors	
Type–diameter–pore size	THC recovery (%)	Type	THC recovery (%)
PTFE–25 mm–0.2 μm	0	PureSal/filtration (swab + squeeze)	7 (±13)
PES–25 mm–0.2 μm	0	NeoSal (swab + buffer) 1 : 4	16 (±5)
PVDF–25 mm–0.2 μm	0	SalivaBio swab (swab + squeeze)	84 (±24)
Nylon–25 mm–0.2 μm	0	SalivaBio swab + pure Sal filter	72 (±20)
Nylon–25 mm–0.45 μm	0	POREX OFCD-100 (no filter)	94 (±3)
Nylon–13 mm–0.45 um	7 (±7)	POREX OFCD-201-SRF (with filter)	64 (±3)
wwPTFE NanoSEP–0.2 μm	9 (±16)	POREX OFCD-100 + glass wool	75 (±5)
wwPTFE NanoSEP–0.45 μm	0	POREX OFCD-100 swab + glass wool	75 (±5)
wwPTFE-13 mm–0.45 μm	0	Centrifuged	91 (±19)
wwPTFE–13 mm–0.2 μm	76 (±20)	N/A	N/A
wwPTFE–25 mm–0.2 um	64 (±7)	N/A	N/A
Glass wool (Pyrex 3950)	76 (±5)	N/A	N/A

[a] PTFE – polytetrafluoroethylene, PES – polyethersulfone, PVDF – polyvinylidene, wwPTFE – water wettable polytetrafluoroethylene.
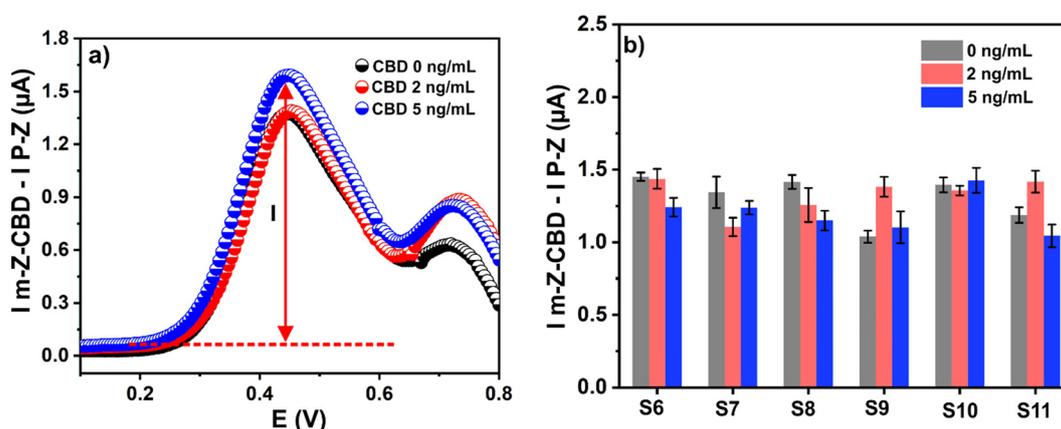
Fig. 4 a) Subtraction signals for the samples (0, 2, and 5 ng mL^{-1} CBD) recovered with m-Z-CBD minus signals obtained with pristine Zensor. b) Sensor electrochemical performance using 100 ng of CBDi and testing synthetic six real saliva samples (S6–S11) with 0, 2, and 5 ng mL^{-1} CBD collected and filtered with OFCD-100 swab/glass wool.

THC (CBD). The impact of CBD on THC detection was studied employing the m-Z-THC sensor, and the effect of THC using the m-Z-CBD sensor when CBD was detected. Fig. 5a illustrates an example of the raw data in detecting THC (2 ng mL^{-1}) in the presence of different amounts of CBD (0, 10, and 50 ng mL^{-1}) using the m-Z-THC sensor. After the analyses, three well-defined peaks appeared between 0.4 and 0.6 V. Furthermore, a shift to higher potential values was observed when 50 ng mL^{-1} CBD was employed as an interferent.

As shown in Fig. 1, the peak for CBD appears at higher potential values compared to THC signals when the electrochemical oxidation of these molecules is carried out; therefore, the presence of CBD in the sample can provoke the change observed in the THC signal potential. Similar signals are observed when THC is present during CBD detection using m-Z-CBD (Fig. 5b). In this case, the three peaks evidenced after analyses appear between 0.4 and 0.6 V. However, the peaks observed when THC was employed as an interferent were broader, and a shift in the potential was observed for both interfering concentrations (10 and 50 ng mL^{-1}). This shift was more significant when 50 ng mL^{-1} THC was employed.

In this research, six samples from different healthy co-workers were employed in the experiments. Fig. 5c shows the results of THC detection in the presence of CBD using the m-Z-THC sensor. However, as can be seen, the signals cannot be differentiated when the sample is analyzed with a different amount of the target analyte and interfering molecule. A similar behaviour is observed when the m-Z-CBD sensor is employed for CBD detection in the presence of THC concentrations (Fig. 5d). The similarities in the chemical structures of THC and CBD and the saliva-to-saliva variation (person-to-person variation) are the two principal factors that lead to the inability to differentiate between the signals obtained from the different performed experiments. However, the influence of these two factors on the final results can be corrected using machine learning.

3.4. Machine learning algorithms

3.4.1. ML as a new tool for analyzing the THC and CBD sensor performances. Random forest (RF), support vector machine (SVM), and artificial neural network (ANN) are the
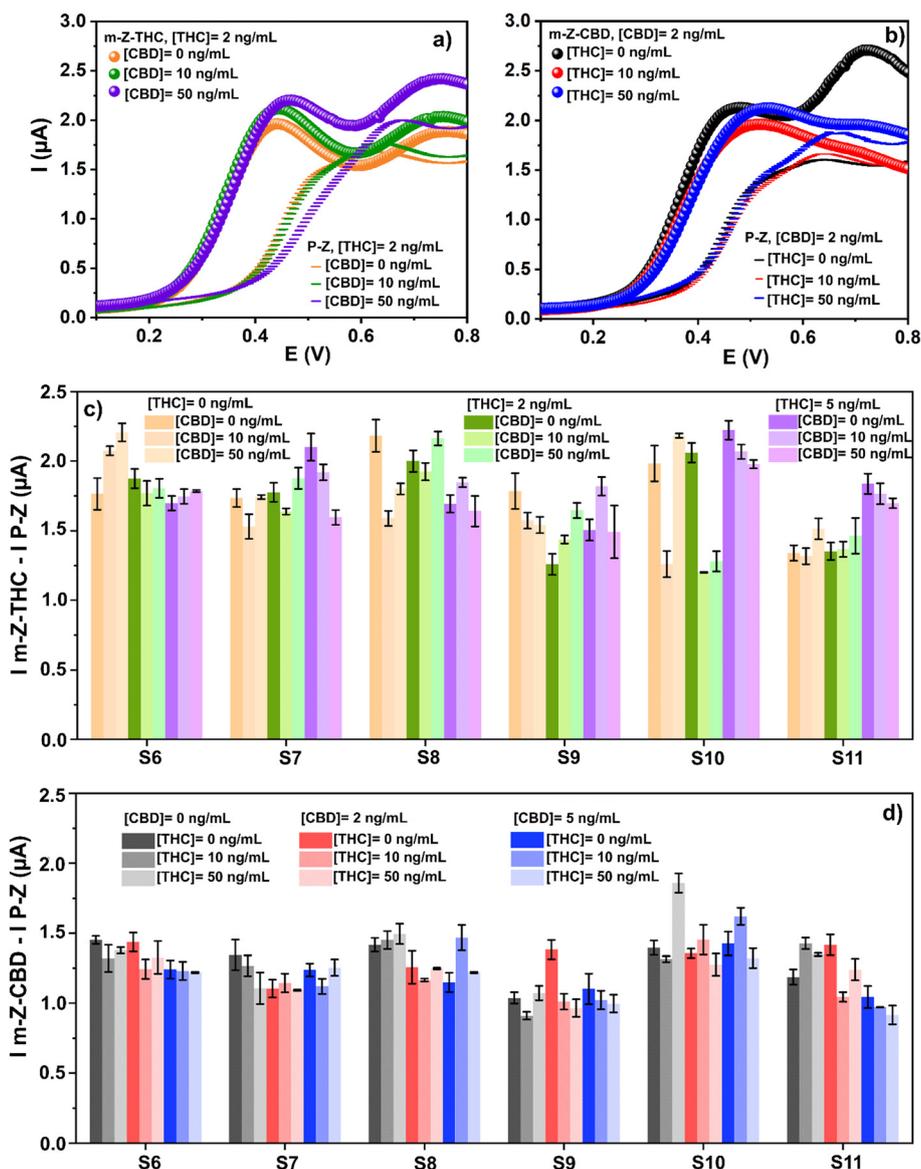
Fig. 5 Square wave voltammetric response of a) m–Z–THC and b) m–Z–CBD sensors for 0, 2, and 5 ng mL^{-1} THC and CBD detection in the presence of interferences (0, 10, and 50 ng mL^{-1} THC or CBD) in human saliva. Subtraction $I_{\text{m-Z-THC}} - I_{\text{p-Z}}$ for c) m–Z THC and d) m–Z–CBD sensors.

three versatile machine learning algorithms that were employed for the classification task. The RF was chosen because a decision tree ensemble algorithm is less prone to overfitting and more explainable due to its rule-based characteristics. Also, RF is less sensitive to feature scaling. SVM was chosen because of the small size of the dataset and the high-dimensionality of the dataset. Finally, ANN was selected because of its ability to handle complex datasets. These methods were applied to datasets with 122 and 181 instances associated with saliva samples comprised of 0, 2, and 5 ng mL^{-1} THC in the first dataset or CBD in the second one. The raw data analyzed using ML resulted in the complete signals obtained after performing the subtraction of the peaks for the samples recovered, *i.e.*, subtracting the signal of the pristine electrode (p-Z) from the signals of the

m-Z-THC or m-Z-CBD electrodes (Fig. 4a). Additional conditions include using the m-Z-THC electrodes with 130 ng of THCi and m-Z-CBD with 100 ng of CBDi and collecting different saliva samples *via* the help of the POREX OFCD-100 + glass wool.

Moreover, proper selection of signal features can play a critical role in the success of a ML model. As a result, ML techniques were trained with only statistical features of signals, including the maximum, minimum, distance between the maximum and the minimum, mean, variance, skewness, and kurtosis or the entire signal (Fig. 3c). Different dimensionality reduction techniques were used on the whole signal. Furthermore, the effect of feature scaling on ML techniques was studied. The datasets for all techniques were split into training and testing.
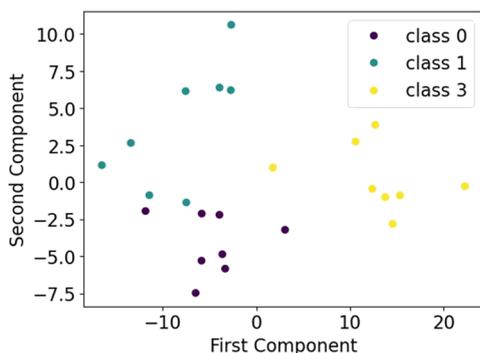
Fig. 6 Distribution of the first and second principal components for a ternary classification of CBD.

The best scenario using statistical features resulted in an accuracy of 100% in training and a poor accuracy of 60% in testing. The norm in most literature studies using training ML techniques only on statistical features is deemed unsuccessful. For this reason, instead of using statistical features, the mentioned RF, SVM, and ANN techniques were applied to the entire signal (Table 2).

The results demonstrate significant improvements in the accuracy of ML techniques with dimensionality reduction and preprocessing. A complex dataset with many features is often susceptible to overfitting and sparsity, where training instances are not distributed uniformly across all dimensions. This indicates that the dataset can be transferred to a lower-dimension space with minimal information leakage (less than 2%). A scatter plot visualizes the relationship of the first two principal components for the multi-classification of CBD for a sample dataset (Fig. 6).

Dimensionality reduction techniques scale down the impact of noise and redundant features, consequently increasing the accuracy. SVM and ANN methods are sensitive to the scale of features and distances between instances. As a result, feature rescaling can improve the performance of the models.

Overall, the RF model with dimensionality reduction outperforms SVM and ANN. This result can be explained based on the nature of the RF technique as an ensemble machine-learning technique. It combines various rule-based decision trees on a random subset of the entire data, where each tree is trained on a random set of features. This randomness curbs the overfitting problem of the decision tree. Moreover, RF is a rule-based technique and is less sensitive to feature scaling. It should be noted that variations in signal shapes represent mainly saliva variation.

3.4.2. ML as a new tool for analyzing the THC and CBD sensor performances in the presence of CBD or THC as an interference. SVM, decision tree, and logistic regression were used to classify signals during THC detection with m-Z-THC without and in the presence of different concentrations of CBD as an interferent. However, considering both THC and CBD resulted in similar SWV responses, implying that the models failed to differentiate the signals. For this reason, and analogously to the experiment described above, CBD detection with m-Z-CBD was performed considering THC as an interference.

Table 3 summarizes the accuracy of each model in training and testing THC and CBD samples interrogated with m-Z-THC and m-Z-CBD and in the presence of cross-interference CBD and THC, respectively. The ML techniques were used to identify signals with interference (class 1) *versus* signals without interference (class 2). The results demonstrate the superiority of the SVM method over other classification techniques. The entire signal features were used for training and preprocessing, including applying dimensionality reduction on datasets before training for all methods except the decision tree.

Table 2 Accuracies of ML techniques trained with the entire signal for m-Z-THC and m-Z-CBD sensors

Model	Preprocessing	Number of principal components		Train		Test	
		THC	CBD	m-Z-THC	m-Z-CBD	m-Z-THC	m-Z-CBD
RF	—	—	—	100	100	76	65
RF	—	12	7	100	100	92	84
SVM	StandardScaler	—	—	78	75	56	62
SVM	—	18	7	83	78	76	62
SVM	PowerTransformer	8	5	99	92	84	78
ANN	—	—	—	82	88	68	68
ANN	StandardScaler	—	—	93	94	83.5	70

Table 3 Results of ML techniques for binary identification of the CBD interferent during testing THC samples with m-Z-THC and the THC interferent during testing CBD samples with m-Z-CBD

Technique	m-Z-THC		m-Z-CBD	
	Training (%)	Testing (%)	Training (%)	Testing (%)
Logistic regression	70	70	68	70
Decision tree	70	72	66	63
Support vector machine	95	90	96	93

Table 4 Results of ML techniques for multi-classification

Sensor	Training (%)	Testing (%)
m-Z-THC	96	77
m-Z-CBD	96	72

The SVM model was used to classify the concentration class of the target sensor in the presence of THC/CBD. Table 4 summarizes the accuracy of results for training and testing datasets for both sensors. The results prove the

capability of the SVM method to identify the class in the presence of an interferent.

Finally, an SVM regression model was deployed to predict the exact concentration of THC in the presence of CBD. Fig. 7 shows a histogram of predicted results per class for training and testing sets. The result is auspicious despite being trained by discrete values and not continuous concentration values. However, since regression does not meet the high standard for accuracies in real THC testing (higher than 90%), it was discarded as a viable option for CBD, and instead, only the SVM classification method was pursued. Although this article
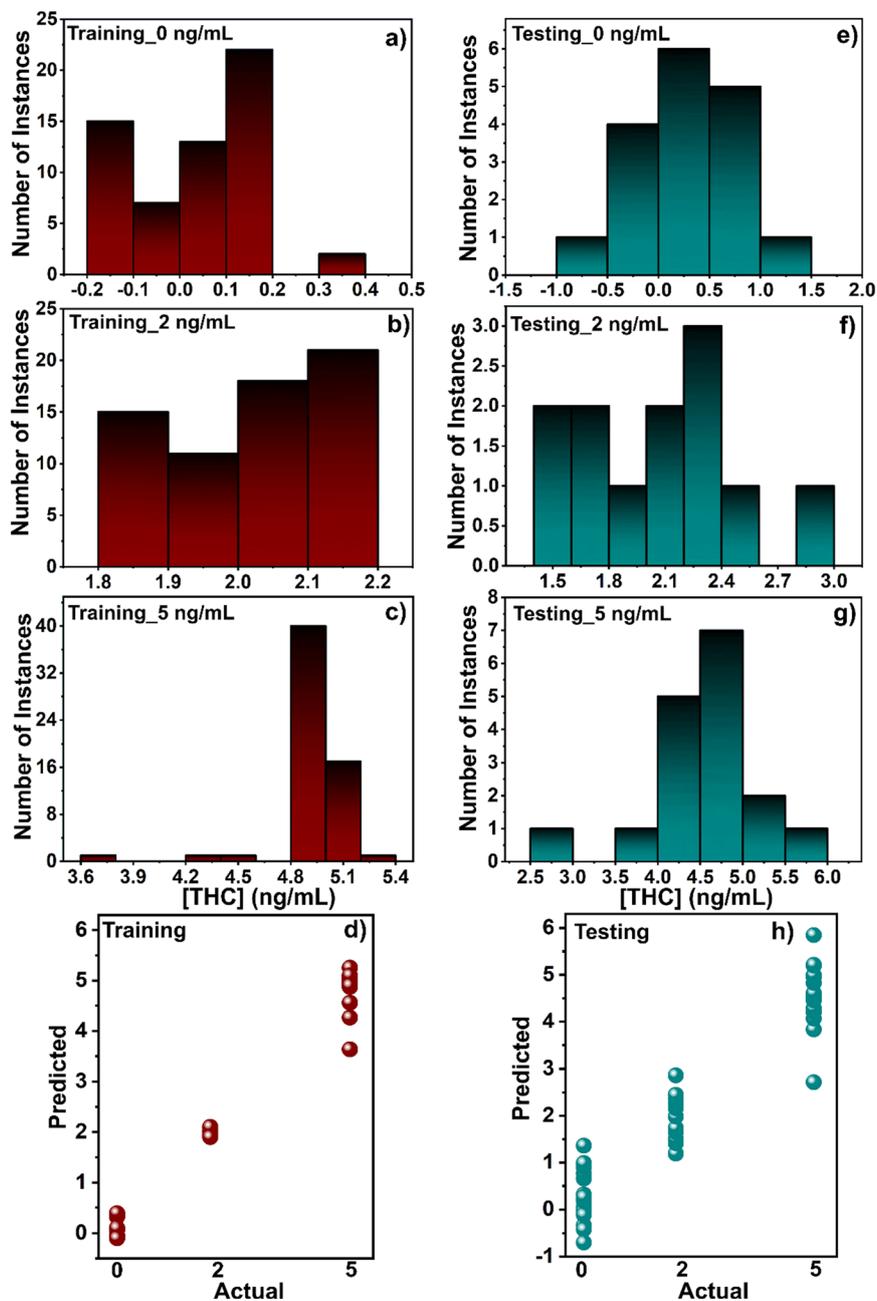
Fig. 7 Histogram of a)–c) training and e)–g) testing results of saliva samples containing THC (0, 2, and 5 ng mL^{-1}) in the presence of CBD and m-Z-THC sensor. Summary of the results of predicted THC concentration vs. actual 0, 2, and 5 ng mL^{-1} for d) training and h) testing ($R^2 = 0.7$).

presents robust classification results, further work is needed to develop a reliable regression model.

4. Conclusions

This work presented electrochemical-based sensors coupled with machine learning analysis for the ultra-low detection of THC or CBD in real saliva samples in the absence or presence of CBD or THC as an interferent. Due to variations in person-to-person saliva and potential CBD/THC interferences, the traditional analysis of calibration curves by plotting analyte concentrations *versus* response current values led to unacceptable results. Therefore, ML algorithms were introduced to analyze the datasets to overcome these setbacks. Overall, the classification of THC (CBD) samples with 0, 2, and 5 ng mL^{-1} presented the best performance, with accuracies approaching 92% and 83% for testing when using RF. In addition, the results proved the capability of ML techniques for identifying the presence of the CBD or THC interference with accuracies of 90–93% and multi-classification with accuracies of 72–77% using SVM.

Ethical statement

All experiments were performed in accordance with the Institution Guidelines, and approved by the ethics committee at McMaster University. Informed consents were obtained from human participants of this study.

Data availability

While we are committed to transparency and publishing the details of the method used in this work, we are constrained by a patent proprietary agreement to publish raw data and code.

Conflicts of interest

There are no conflicts to declare.

Acknowledgements

References

1 M. Klimuntowski, M. M. Alam, G. Singh and M. M. R. Howlader, *ACS Sens.*, 2020, **5**, 620–636.

2 G. Pearlson, *Weed Sci.*, 2020, 246–260.

3 G. A. Ortega, S. R. Ahmed, S. K. Tuteja, S. Srinivasan and A. R. Rajabzadeh, *Talanta*, 2022, **236**, 122863.

4 V. Ramzy and R. Priefer, *Talanta*, 2021, **222**, 121528.

5 M. A. Balbino, I. C. Eleotério, L. S. De Oliveira, M. M. T. De Menezes, J. F. De Andrade, A. J. Ipólito and M. F. De Oliveiraa, *J. Braz. Chem. Soc.*, 2014, **25**, 589–596.

6 T. Pholsiri, A. Lomae, K. Pungjunun, S. Vimolmangkang, W. Siangproh and O. Chailapakul, *Sens. Actuators, B*, 2022, **355**, 131353.

7 B. Zanfrognini, L. Pigani and C. Zanardi, *J. Solid State Electrochem.*, 2020, **24**, 2603–2616.

8 X. Tang, Y. Gu, P. Tang and L. Liu, *Int. J. Electrochem. Sci.*, 2022, **17**, 220562.

9 H. Luo, L. X. Chen, Q. M. Ge, M. Liu, Z. Tao, Y. H. Zhou and H. Cong, *J. Inclusion Phenom. Macrocyclic Chem.*, 2019, **95**, 171–198.

10 A. Khoobi, N. Soltani and M. Aghaei, *J. Alloys Compd.*, 2020, **831**, 154715.

11 R. G. Rocha, J. S. Stefano, I. V. S. Arantes, M. M. A. C. Ribeiro, M. H. P. Santana, E. M. Richter and R. A. A. Munoz, *Electroanalysis*, 2019, **31**, 153–159.

12 A. Gomez Cardoso, S. Rahin Ahmed, Z. Keshavarz-Motamed, S. Srinivasan and A. Reza Rajabzadeh, *Bioelectrochemistry*, 2023, **152**, 108440.

13 A. G. Cardoso, H. Viltres, G. A. Ortega, V. Phung, R. Grewal, H. Mozaffari, S. R. Ahmed, A. R. Rajabzadeh and S. Srinivasan, *TrAC, Trends Anal. Chem.*, 2023, **160**, 116965.

14 K. Ngamchuea, C. Batchelor-McAuley and R. G. Compton, *Sens. Actuators, B*, 2018, **262**, 404–410.

15 C. Pezzo, *Hands-On Machine Learning with Scikit-Learn & TensorFlow*, 2017.

16 M. Mohri, A. Rostamizadeh and A. Talwalkar, *Foundations of Machine Learning*, 2nd edn, 2012.

17 Y. Nakano, T. Takeshita, N. Kamio, S. Shiota, Y. Shibata, N. Suzuki, M. Yoneda, T. Hirofuji and Y. Yamashita, *Artif. Intell. Med.*, 2014, **60**, 97–101.

18 Ö. B. Mercan, V. Kılıç and M. Şen, *Sens. Actuators, B*, 2021, **329**, 129037.

19 A. Carrio, C. Sampedro, J. L. Sanchez-Lopez, M. Pimienta and P. Campoy, *Sensors*, 2015, **15**, 29569–29593.

20 P. C. Riley and S. V. Deshpande, Machine learning based spectral interpretation in chemical detection, *Proc. SPIE 11006, Artificial Intelligence and Machine Learning for Multi-Domain Operations Applications*, 10 May 2019, p. 110061X, DOI: **10.1117/12.2518929**.

21 D. Ding, S. Han, H. Zhang, Y. He and Y. Li, *Comput. Biol. Chem.*, 2019, **83**, 107106.

22 M. Sánchez-Brito, F. J. Luna-Rosas, R. Mendoza-González, M. M. Mata-Miranda, J. C. Martínez-Romo and G. J. Vázquez-Zapién, *Talanta*, 2021, **221**, 121650.

23 M. Ghassemi, S. Barzegari, P. Hajian, H. Zham, H. R. Mirzaei and F. H. Shirazi, *J. Mol. Struct.*, 2021, **1229**, 129493.

24 P. Puthongkham, S. Wirojsaengthong and A. Suea-Ngam, *Analyst*, 2021, **146**, 6351–6364.

25 I. Strauss, G. Valle, F. Artoni, E. D'Anna, G. Granata, R. Di Iorio, D. Guiraud, T. Stieglitz, P. M. Rossini, S. Raspopovic, F. M. Petrini and S. Micera, *Sci. Rep.*, 2019, **9**, 1–11.

26 S. I. Hwang, N. G. Franconi, M. A. Rothfuss, K. N. Bocan, L. Bian, D. L. White, S. C. Burkert, R. W. Euler, B. J. Sopher, M. L. Vinay, E. Sejdic and A. Star, *ACS Sens.*, 2019, **4**, 2084–2093.

27 Z. Rao, B. Guo, J. Zu, W. Zheng and Y. Zu, *IEEE Sens. J.*, 2024, **24**, 7463–7472.

28 D. Caprioglio, D. Mattoteia, O. Taglialatela-Scafati, E. Muñoz and G. Appendino, *Biomolecules*, 2021, **11**, 991.

29 H. Hantsche, *Adv. Mater.*, 1993, **5**, 778.

30 M. Biesninger, X-ray Photoelectron Spectroscopy (XPS) Reference Pages, (accessed 28 September 2023).

31 H. Viltres, O. F. Odio, M. C. Biesinger, G. Montiel, R. Borja and E. Reguera, *ChemistrySelect*, 2020, **5**, 4875–4884.